IEEE Access
Multidisciplinary | Rapid Review | Open Access Journal

Received May 9, 2020, accepted June 9, 2020, date of publication June 19, 2020, date of current version July 1, 2020.

Digital Object Identifier 10.1109/ACCESS.2020.3003754

Impedance Network Model of D-PMSG Based Wind Power Generation System Considering Wind Speed Variation for Sub-Synchronous Oscillation Analysis

SHUN TAO[1], (Member, IEEE), LEI ZHAO[1], YUNBO LIU[1], AND KUNYU LIAO[2]
[1]State Key Laboratory for Alternate Electrical Power System with Renewable Energy Sources, North China Electric Power University, Beijing 102206, China
[2]Suzhou Power Supply Company, State Grid Jiangsu Electric Power Company Ltd., Suzhou 215004, China

Corresponding author: Lei Zhao (zhaoleicyjx@163.com)

This work was supported by the National Natural Science Foundation of China under Grant 51777066.

ABSTRACT Recently, sub-synchronous oscillation (SSO) issues were observed in direct-drive permanent magnet synchronous generator (D-PMSG) based wind power generation systems (WPGS) comprising multiple wind farms. Impedance model (IM) analysis has become an important method to study such problems. In this paper, an IM of a D-PMSG grid-connected system (GCS) is established considering the relationship between wind speed and wind turbine output power and the effect of voltage outer loop control. An impedance network model (INM) for a multi-wind-farm grid-connected system (MWFGS) is constructed with IMs of each wind turbine/farm and transmission lines according to the interconnection topology of them. Then, based on the IM of the D-PMSG-GCS, the influence of wind speed on the SSO characteristics is quantitatively analyzed, and the accuracy of the model is verified by comparing with the eigenvalue analysis results. Finally, the influencing factors such as distributed wind speed and network topology of MWFGS on SSO characteristics are quantitatively analyzed based on the INM, and the time-domain simulation verifications are performed in PSCAD/EMTDC. The results prove the effectiveness of INM in analyzing SSO problems of a large-scale WPGS. This is of great significance for the planning of large-scale D-PMSG-based WPGSs and the suppression of SSO.

INDEX TERMS Direct-drive permanent magnet synchronous generator (D-PMSG), sub-synchronous oscillation (SSO), impedance network model (INM), wind speed, voltage outer loop.

NOMENCLATURE

SSO	Sub-synchronous oscillation
D-PMSG	Direct-drive permanent magnet synchronous generator
WPGS	Wind power generation systems
GCS	Grid-connected system
MSC	Machine-side converter
INM	Impedance network model
MWFGS	Multi-wind-farm grid-connected system
WT	Wind turbine
PLL	Phase-locked loop
MPPT	Maximum power point tracking
WF	Wind farm
PCC	Point of common coupling

The associate editor coordinating the review of this manuscript and approving it for publication was Jenny Mahoney.

I. INTRODUCTION

As a green renewable energy resource, wind power has played an important role in solving the current global energy crisis and environmental pollution problems [1]. However, in recent years, problems related to the oscillation stability of wind turbines have occurred in many regions of China. In July 2015, the severe sub-synchronous oscillation (SSO) without series compensation occurred in the wind farm based on D-PMSGs in Hami area of Xinjiang, China [2], [3].

At present, the time-domain simulation method [4], the eigenvalue method [5], [6], and the impedance model method [7]–[16] have been used for the research of SSO issues. However, for the SSO analysis of a large-scale WPGS, the time-domain simulation method is time-consuming, and the eigenvalue method will face the problem of ''dimensional disaster'' [7]. Because the impedance model analysis method has the advantages of clear physical concepts and strong

scalability, it is suitable for analyzing the SSO problems of a large-scale WPGS.

There are two main ideas for impedance modeling of power electronic converters. One is to establish the sequence impedance model of a converter in the abc three-phase stationary coordinate system [8], [9], and the other is to establish the impedance model in the dq synchronous rotation coordinate system [7], [16]. The sequence impedance model represents a one-dimensional impedance, but in the process of modeling, the effects of positive and negative sequence coupling, voltage outer loop control, AC-DC dynamic coupling, and asymmetry of the parameters of the dq-axis controllers are ignored, making precise modeling difficult. Based on the 2*2 order impedance matrix model in the dq coordinate system, the problems such as dq axis coupling can be easily solved.

The voltage outer loop control has a significant impact on the dynamic characteristics of the lower frequency range of the system [13]–[16]. Reference [16] considered the voltage outer loop control, but did not quantify the stability of the renewable energy system; [7] proposed a quantitative method for stability analysis, but did not give the expression of corresponding impedance model.

Wind speed is one of the important factors affecting the grid-connected operation of D-PMSGs [2], [17], [18]. Though [2] qualitatively pointed out the impact of wind turbine (WT) output power on the SSO characteristics, it did not give a model for quantitative analysis. Reference [18] quantified the influence of wind speed on the SSO characteristics of a D-PMSG based WPGS based on the eigenvalue analysis. However, there is no literature to quantify the impact of wind speed on the SSO characteristics of D-PMSG based WPGS with impedance model analysis method.

Existing IMs of a D-PMSG based WPGS are simplified ''single-machine-infinite-bus'' system models [9], [16], [20]. That is, the wind farm is aggregated into one WT or many identical WTs are connected to a common bus, and the power network is reduced to an equivalent series line. However, an actual large-scale WPGS usually consists of multiple geographically distributed wind farms, and each wind farm contains different numbers and types of WTs. Moreover, due to the distributed wind speed, their operating conditions will be diversified. The simplified '' single-machine-infinite-bus '' system model is difficult to characterize a real WPGS including multiple wind farms with different WTs. It cannot reflect the influence of the key factors such as network topology, spatial distribution of wind farms, diversity of WTs and distributed wind speed on SSO characteristics. In [23], considering the above factors, an INM was proposed to analyze the stability of the sub-synchronous resonance of the multiple wind farms series compensation system, but the impedance model expression of the D-PMSG was not presented.

In this paper, an IM of a D-PMSG-GCS is first established considering the effects of voltage outer loop, current inner loop, phase-locked loop, DC dynamic link and filtering, and wind speed is introduced into the model utilizing the function of wind turbine output power. An INM for an MWFGS is constructed with IMs of each wind turbine/farm and transmission lines according to the interconnection topology of them. Then, based on the IM of the D-PMSG-GCS, the influence of wind speed on the SSO characteristics is quantitatively analyzed, and the accuracy of the model is verified by comparing with the eigenvalue analysis results. Finally, the influencing factors such as distributed wind speed and network topology of MWFGS on SSO characteristics are quantitatively analyzed based on the INM, and the time-domain simulation verifications are performed in PSCAD/EMTDC. The results prove the effectiveness of INM in analyzing SSO problems of a large-scale WPGS. This is of great significance for the planning of a large-scale D-PMSG based WPGS and the suppression of SSO.

II. D-PMSG EQUIVALENT CIRCUIT AND CONTROL SYSTEM

A D-PMSG mainly consists of a WT, a PMSG, a machine-side converter (MSC), a grid-side converter (GSC), a DC link, and an L filter [2], [24]. The DC link separates MSC and GSC without affecting each other, and the on-grid dynamics of a D-PMSG mainly depends on the control features of its GSC [2]. Therefore, a D-PMSG is generally equivalent to a voltage source converter (VSC) [8], [9], [16], as shown in Fig. 1.

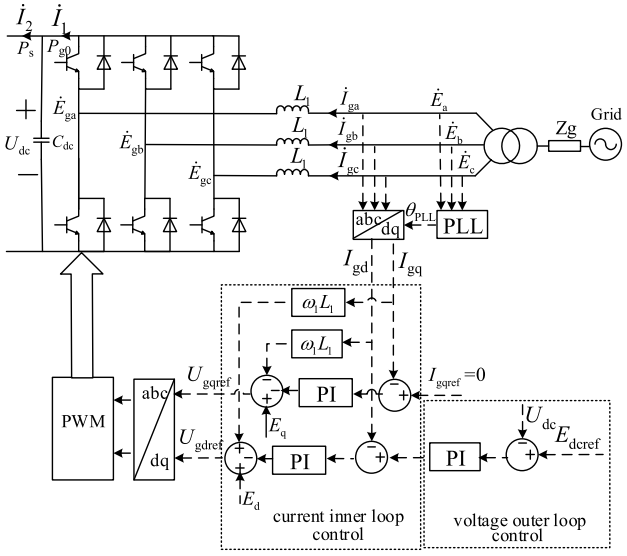

FIGURE 1. D-PMSG grid side main circuit and control system.

Fig. 1 consists of two parts: the equivalent circuit and the control loops. The GSC of the D-PMSG is connected to the infinite grid through a filter link L_1, a transformer, and a grid connection impedance Z_g. The current reference direction is from the grid to the PMSG [16]. The control loops including the voltage outer loop, the current inner loop, and the phase-locked loop (PLL), are oriented at the grid voltage in the dq frame system. The controllers of the current inner loop

and the voltage outer loop adopt the proportional-integral (PI) controls.

III. MODELING THE IM OF THE D-PMSG-GCS

The IM of the D-PMSG-GCS is established in the form of per-unit value. Besides the considerations of the voltage outer loop, the current inner loop, the phase-locked loop and etc., the model takes a wind speed variable into account by using the functional relationship between wind speed and output power of WT, to accurately quantify the influences of wind speed on the SSO frequency and damping of the system.

For the convenience of the following model deduction, there are two equivalents to represent the electrical quantities in Fig. 1: one is the vector form like $\mathbf{E} = E_\mathrm{d} + jE_\mathrm{q}$, the other is the scalar form like $\mathbf{E} = \begin{bmatrix} E_\mathrm{d} & E_\mathrm{q} \end{bmatrix}^\mathrm{T}$.

A. IM OF D-PMSG

1) VSC AC SIDE DYNAMIC LINK

As shown in Fig. 1, the dynamic equation of the GSC AC-side circuit is,

$$(\frac{s}{\omega_\mathrm{b}}L_1 + j\omega_1 L_1)\mathbf{I_g} = \mathbf{E} - \mathbf{U_g} \tag{1}$$

where, L_1 is in p.u, ω_b is the base angular frequency in rad/s, ω_1 is the base angular frequency in p.u, $\mathbf{I_g}$ is the vector of the output current, and $\mathbf{E}$ is the voltage vector of the point of common coupling (PCC), $\mathbf{U_g}$ is the vector of inverter output voltage.

2) CURRENT INNER LOOP

In the current inner loop, the unit power factor control mode is used, that is, $I_\mathrm{gqref} = 0$ [6]–[10].

According to Fig.1, the current inner loop control equation is,

$$\mathbf{U_{gref}} = -\underbrace{(k_{gi} + \frac{1}{T_\mathrm{gi}s})}_{F_\mathrm{I}(s)}(\mathbf{I_{gref}} - \mathbf{I_g}) - j\omega_1 L_1 \mathbf{I_g} + \mathbf{E} \tag{2}$$

where, $\mathbf{U_{gref}}$ is the reference vector of the GSC output voltage, $\mathbf{I_{gref}}$ is the reference vector of the output current, and k_gi and T_gi are the proportional gain coefficient and the integration time constant of the PI controller, respectively.

The equation for the modulation link is

$$\begin{aligned} \mathbf{U_g} &= U_\mathrm{dcb}/2/U_\mathrm{phb}U_\mathrm{dc}\mathbf{U_{gref}} \\ &= kU_\mathrm{dc}\mathbf{U_{gref}} \end{aligned} \tag{3}$$

where, U_dcb is the DC voltage base value, U_phb is the AC voltage base value, U_dc is the DC side voltage, and k is the GSC output voltage gain.

3) VOLTAGE OUTER LOOP

As shown in Fig. 1, the voltage outer loop control equation is,

$$I_\mathrm{gdref} = \underbrace{(k_\mathrm{gu} + \frac{1}{T_\mathrm{gu}s})}_{F_\mathrm{dc}(s)}(E_\mathrm{dcref} - U_\mathrm{dc}) \tag{4}$$

where, k_gu and T_gu are the proportional gain coefficient and the integration time constant of the voltage outer loop controller, respectively, E_dcref is the reference value of DC voltage, and I_gdref is the reference value of d-axis current.

Equation (5) is obtained based on (1)-(4) and presented into a matrix form.

$$\begin{aligned} &\begin{bmatrix} \frac{s}{\omega_\mathrm{b}}L_1 + kU_\mathrm{dc}F_\mathrm{I}(s) & kU_\mathrm{dc}\omega_1 L_1 - \omega_1 L_1 \\ \omega_1 L_1 - kU_\mathrm{dc}\omega_1 L_1 & \frac{s}{\omega_\mathrm{b}}L_1 + kU_\mathrm{dc}F_\mathrm{I}(s) \end{bmatrix} \begin{bmatrix} I_\mathrm{gd} \\ I_\mathrm{gq} \end{bmatrix} \\ &= \begin{bmatrix} 1 - kU_\mathrm{dc} & 0 \\ 0 & 1 - kU_\mathrm{dc} \end{bmatrix} \begin{bmatrix} E_\mathrm{d} \\ E_\mathrm{q} \end{bmatrix} \\ &\quad + kU_\mathrm{dc}F_\mathrm{I}(s) \begin{bmatrix} F_\mathrm{dc}(s)(E_\mathrm{dcref} - U_\mathrm{dc}) \\ 0 \end{bmatrix} \end{aligned} \tag{5}$$

Equation (6) is obtained by adding a small disturbance at the PCC based on (5).

$$\begin{aligned} &\begin{bmatrix} A & B \\ -B & A \end{bmatrix} \begin{bmatrix} I_\mathrm{gd0} + \Delta I_\mathrm{gd} \\ I_\mathrm{gq0} + \Delta I_\mathrm{gq} \end{bmatrix} \\ &= \begin{bmatrix} C & 0 \\ 0 & C \end{bmatrix} \begin{bmatrix} E_\mathrm{d0} + \Delta E_\mathrm{d} \\ E_\mathrm{q0} + \Delta E_\mathrm{q} \end{bmatrix} + (U_\mathrm{dc0} + \Delta U_\mathrm{dc}) \begin{bmatrix} D \\ 0 \end{bmatrix} \end{aligned} \tag{6}$$

where, ΔU_dc is the deviation of the DC voltage, and U_dc0 is the per-unit value of the DC voltage in steady-state,

$$\begin{cases} A = \frac{s}{\omega_\mathrm{b}}L_1 + k(U_\mathrm{dc0} + \Delta U_\mathrm{dc})F_\mathrm{I}(s) \\ B = k(U_\mathrm{dc0} + \Delta U_\mathrm{dc})\omega_1 L_1 - \omega_1 L_1 \\ C = 1 - k(U_\mathrm{dc0} + \Delta U_\mathrm{dc}) \\ D = kF_\mathrm{I}(s)F_\mathrm{dc}(s)(E_\mathrm{dcref} - (U_\mathrm{dc0} + \Delta U_\mathrm{dc})). \end{cases}$$

The small-signal model (7) is obtained by linearizing (6).

$$\begin{aligned} &\begin{bmatrix} E & F \\ -F & E \end{bmatrix} \begin{bmatrix} I_\mathrm{gd0} \\ I_\mathrm{gq0} \end{bmatrix} + \begin{bmatrix} G & H \\ -H & G \end{bmatrix} \begin{bmatrix} \Delta I_\mathrm{gd} \\ \Delta I_\mathrm{gq} \end{bmatrix} \\ &= \begin{bmatrix} J & 0 \\ 0 & J \end{bmatrix} \begin{bmatrix} E_\mathrm{d0} \\ E_\mathrm{q0} \end{bmatrix} + \begin{bmatrix} K & 0 \\ 0 & K \end{bmatrix} \begin{bmatrix} \Delta E_\mathrm{d} \\ \Delta E_\mathrm{q} \end{bmatrix} - \Delta U_\mathrm{dc} \begin{bmatrix} M \\ 0 \end{bmatrix} \end{aligned} \tag{7}$$

where

$$\begin{cases} E = k\Delta U_\mathrm{dc}F_\mathrm{I}(s) \\ F = k\Delta U_\mathrm{dc}\omega_1 L_1 \\ G = \frac{s}{\omega_\mathrm{b}}L_1 + kU_\mathrm{dc0}F_\mathrm{I}(s) \\ H = kU_\mathrm{dc0}\omega_1 L_1 - \omega_1 L_1 \\ J = -k\Delta U_\mathrm{dc} \\ K = 1 - kU_\mathrm{dc0} \\ M = kF_\mathrm{I}(s)U_\mathrm{dc0}F_\mathrm{dc}(s). \end{cases}$$

Take the grid voltage as the orientation vector of the vector control system, that is, set the grid voltage vector $\mathbf{E}$ on the d-axis in the synchronous rotation coordinate system, and then rotate it 90° counterclockwise to obtain the q-axis, then

$$\begin{cases} E_\mathrm{d} = E_0 \\ E_\mathrm{q} = 0 \end{cases} \tag{8}$$

where E_0 is the voltage of PCC at a steady-state operating point. The following electrical variables with the subscripts containing 0 are the values at the steady-state operating point.

After considering small disturbances, the vectors of the GSC output voltage and the inductor current are $\mathbf{U_g} = (U_{gd0}+\Delta U_{gd}) + j(\mathrm{U}_{gq0} + \Delta \mathrm{U}_{gq})$ and $\mathbf{I_g} = \left(I_{gd0} + \Delta I_{gd}\right) + j\left(I_{gq0} + \Delta I_{gq}\right)$ respectively. Therefore, the complex power transmitted by GSC is $\mathbf{S} = \mathbf{U_g}\mathbf{I}_g^* = P_g + jQ_g$, and then

$$\begin{cases} \Delta P_g = I_{gd0}\Delta U_{gd} + I_{gq0}\Delta U_{gq} + U_{gd0}\Delta I_{gd} + U_{gq0}\Delta I_{gq} \\ \Delta Q_g = I_{gd0}\Delta U_{gq} - I_{gq0}\Delta U_{gd} - U_{gd0}\Delta I_{gq} + U_{gq0}\Delta I_{gd} \end{cases} \tag{9}$$

where the d-axis current at the steady-state operating point is $I_{gd0} = P_{g0}/U_{gd0}$.

The dynamic equation of the DC capacitor is (10) [14].

$$\Delta P_g = \frac{s}{\omega_b}\Delta U_{dc} U_{dc0} C_{dc} \tag{10}$$

where C_{dc} is the per-unit value of the DC-side capacitance.

From (9) and (10), the DC voltage deviation is obtained.

$$\Delta U_{dc} = \frac{I_{gd0}\Delta U_{gd} + I_{gq0}\Delta U_{gq} + U_{gd0}\Delta I_{gd} + U_{gq0}\Delta I_{gq}}{\frac{s}{\omega_b}U_{dc0}C_{dc}} \tag{11}$$

The relationship between $\mathbf{U_g}$ and $\mathbf{E}$ is shown in (1). Therefore, the $\mathbf{U_g}$ at the steady state operating point and its small deviation expressions are shown in (12) and (13), respectively.

$$\begin{cases} U_{gd0} = E_{d0} - \frac{s}{\omega_b}L_1 I_{gd0} + \omega_1 L_1 I_{gq0} \\ U_{gq0} = E_{q0} - \omega_1 L_1 I_{gd0} + \frac{s}{\omega_b}L_1 I_{gq0} \end{cases} \tag{12}$$

$$\begin{cases} \Delta U_{gd} = \Delta E_d - \frac{s}{\omega_b}L_1 \Delta I_{gd} + \omega_1 L_1 \Delta I_{gq} \\ \Delta U_{gq} = \Delta E_q + \frac{s}{\omega_b}L_1 \Delta I_{gq} - \omega_1 L_1 \Delta I_{gd} \end{cases} \tag{13}$$

Because of the zero reactive power control, $I_{gqref} = I_{gq0} = 0$, so (12) can be simplified to (14).

$$\begin{cases} U_{gd0} = E_{d0} \\ U_{gq0} = E_{q0} - \omega_1 L_1 I_{gd0} \end{cases} \tag{14}$$

According to (14), $I_{gd0} = P_{g0}/E_{d0}$.

Equation (15) is obtained by taking (13) and (14) into (11).

$$\Delta U_{dc} = \frac{\Delta E_d I_{gd0} + F_c(s)\Delta I_{gd}}{F_b(s)} \tag{15}$$

where $\begin{cases} F_b(s) = \frac{s}{\omega_b}U_{dc0}C_{dc} \\ F_c(s) = E_{d0} - \frac{sP_{g0}}{\omega_b E_0}L_1 \end{cases}$.

Equation (16) is obtained by taking (15) into (6).

$$\begin{bmatrix} N & H \\ T & G \end{bmatrix}\begin{bmatrix} \Delta I_{gd} \\ \Delta I_{gq} \end{bmatrix} = \begin{bmatrix} X & O \\ W & K \end{bmatrix}\begin{bmatrix} \Delta E_d \\ \Delta E_q \end{bmatrix} \tag{16}$$

where

$$\begin{cases} N = \frac{kF_I(s)P_{g0}}{F_b(s)E_{d0}}F_c(s) + \frac{kE_{d0}F_c(s)}{F_b(s)} + \frac{s}{\omega_b}L_1 \\ \quad + \frac{kF_I(s)U_{dc0}F_{dc}(s)F_c(s)}{F_b(s)} + kF_I(s)U_{dc0} \\ T = -\frac{k\omega_1 L_1 F_c(s)P_{g0}}{F_b(s)E_{d0}} - H \\ X = K - \frac{kP_{g0}}{F_b(s)} - \frac{MP_{g0}}{F_b(s)E_{d0}} - \frac{kF_I(s)P_{g0}P_{g0}}{F_b(s)E_{d0}E_{d0}} \\ O = 0 \\ W = \frac{k\omega_1 L_1 P_{g0}P_{g0}}{F_b(s)E_{d0}E_{d0}} \end{cases}.$$

4) PHASE-LOCKED LOOP

The phase-locked loop control structure is shown in Fig. 2.

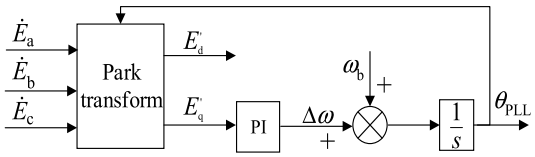

FIGURE 2. Phase-locked loop control structure.

As shown in Fig. 2, the control equation of the PLL is,

$$\Delta\omega = \underbrace{(K_{pp} + \frac{1}{sT_{ip}})}_{F_{PLL}(s)}E'_q \tag{17}$$

$$\frac{d\theta_{PLL}}{dt} = \omega_b + \Delta\omega \tag{18}$$

where $\Delta\omega$ is the difference between the PLL output angular frequency and the actual grid voltage angular frequency, and K_{pp} and T_{ip} are the proportional gain coefficient and the integration time constant of the PLL controller, respectively. E'_q is the q-axis voltage component obtained by transforming the three-phase voltage at the PCC through the Park transformation after considering the effect of PLL. θ_{PLL} is the output angle of the PLL.

$\Delta\theta = \theta_{PLL} - \theta_s$, and θ_s is the actual grid voltage angle. The voltage phasor at PCC can be expressed as,

$$\begin{aligned} \mathbf{E}' &= e^{-j\Delta\theta}\mathbf{E} = [\cos(\Delta\theta) - j\sin(\Delta\theta)](E_0 + \Delta\mathbf{E}) \\ &\approx E_0 + \Delta\mathbf{E} - jE_0\Delta\theta \end{aligned} \tag{19}$$

Equation (20) can be obtained according to (17)-(19).

$$\frac{d\Delta\theta}{dt} = F_{PLL}(s)(\Delta E_q - E_0\Delta\theta) \tag{20}$$

The transfer function of the PLL can be obtained according to (20).

$$\begin{aligned} \Delta\theta &= \frac{F_{PLL}(s)}{s + F_{PLL}(s)E_0}\Delta E_q \\ &= G_{PLL}(s)\Delta E_q \end{aligned} \tag{21}$$

The schematic diagram of the phase-locked loop is shown in Fig. 3. From Fig. 3, the small deviations of the voltage and

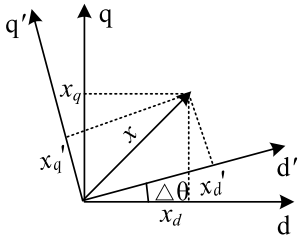

FIGURE 3. Phase-locked loop schematic diagram.

the current at PCC considering the PLL are obtained as shown in (22) and (23), respectively.

$$\begin{bmatrix} \Delta E_{\mathrm{d}}^{'} \\ \Delta E_{\mathrm{q}}^{'} \end{bmatrix} = \begin{bmatrix} \Delta E_{\mathrm{d}} \\ \Delta E_{\mathrm{q}} \end{bmatrix} + \begin{bmatrix} 0 & G_{\mathrm{PLL}}(s)E_{\mathrm{q0}} \\ 0 & -G_{\mathrm{PLL}}(s)E_{\mathrm{d0}} \end{bmatrix} \begin{bmatrix} \Delta E_{\mathrm{d}}^{'} \\ \Delta E_{\mathrm{q}}^{'} \end{bmatrix} \tag{22}$$

$$\begin{bmatrix} \Delta I_{\mathrm{d}}^{'} \\ \Delta I_{\mathrm{q}}^{'} \end{bmatrix} = \begin{bmatrix} \Delta I_{\mathrm{d}} \\ \Delta I_{\mathrm{q}} \end{bmatrix} + \begin{bmatrix} 0 & G_{\mathrm{PLL}}(s)I_{\mathrm{q0}} \\ 0 & -G_{\mathrm{PLL}}(s)I_{\mathrm{d0}} \end{bmatrix} \begin{bmatrix} \Delta E_{\mathrm{d}}^{'} \\ \Delta E_{\mathrm{q}}^{'} \end{bmatrix} \tag{23}$$

Therefore, the equivalent impedance expression (24) of the D-PMSG is obtained by taking (22) and (23) into (16).

$$\begin{aligned} \mathbf{Z}_{\mathrm{w}}(s) &= \begin{bmatrix} X & -HG_{\mathrm{PLL}}\dfrac{P_{\mathrm{g0}}}{E_{d0}} \\ W & K + KG_{\mathrm{PLL}}E_{\mathrm{d0}} - GG_{\mathrm{PLL}}\dfrac{P_{\mathrm{g0}}}{E_{\mathrm{d0}}} \end{bmatrix}^{-1} \\ &\quad \times \begin{bmatrix} N & H \\ T & G \end{bmatrix} \\ &= \begin{bmatrix} Z_{\mathrm{dd}} & Z_{\mathrm{dq}} \\ Z_{\mathrm{qd}} & Z_{\mathrm{qq}} \end{bmatrix} \end{aligned} \tag{24}$$

5) IM OF D-PMSG CONSIDERING WIND SPEED VARIATION

The actual active power obtained by the wind turbine P_{tur} is closely related to the wind speed v, and the relationship is as follows [24]–[26],

$$P_{\mathrm{tur}} = \begin{cases} 0, & v \in [0, v_{\mathrm{cut\text{-}in}}) \\ 0.5\pi R_{\mathrm{tur}}^2 \rho C_{\mathrm{p}} v^3 = k_1 v^3, & v \in [v_{\mathrm{cut\text{-}in}}, v_{\mathrm{rated}}] \\ P_{\mathrm{rate}}, & v \in (v_{\mathrm{rated}}, v_{\mathrm{cut\text{-}out}}] \end{cases} \tag{25}$$

where R_{tur} is the radius of the WT blade, ρ is the air density, $v_{\mathrm{cut-in}}$ is the cut-in wind speed, v_{rated} is the rated wind speed, $v_{\mathrm{cut-out}}$ is the cut-out wind speed, P_{rate} is the rated power of the D-PMSG. C_{p} is the wind energy utilization coefficient, which is kept at the maximum value and constant (generally 0.593) by maximum power point tracking (MPPT). The blade radius of the WT is a constant and the air density is normally assumed as a constant in the same area, thus k_1 in (25) is a constant coefficient.

Considering the power loss of the PMSG and the MSC, the conversion efficiency is assumed as a constant value k_2. Thus, the active power transmitted from the MSC to the DC bus is $P_{\mathrm{s}} = k_2 P_{\mathrm{tur}}$. Ignoring the DC side resistance, it is assumed that the active power is transmitted from the DC bus to the GSC without any loss, that is, $P_{\mathrm{g0}} = P_{\mathrm{s}}$ at the steady-state. P_{g0} in p.u is,

$$P_{\mathrm{g0}} = -k_2 P_{\mathrm{tur}}/S_{\mathrm{b}} \tag{26}$$

where S_{b} is the capacity base value of the system.

By introducing (26) into (24), the equivalent impedance model $\mathbf{Z_{wv}}(s)$ of the D-PMSG considering wind speed variation is obtained.

B. IM OF D-PMSG-GCS

In the abc three-phase stationary coordinate system, the AC grid connection impedance model in D-PMSG-GCS shown in Fig. 1 is expressed as:

$$Z_{\mathrm{g\text{-}abc}} = r_{\mathrm{g}} + \frac{s}{\omega_{\mathrm{b}}} L_{\mathrm{g}} \tag{27}$$

where r_{g} is the AC grid connection resistance in p.u and L_{g} is the AC grid connection inductance in p.u.

Transform the AC grid connection impedance $Z_{\mathrm{g-abc}}$ in (27) into the dq synchronous rotation coordinate system as

$$\mathbf{Z_g}(s) = \begin{bmatrix} r_{\mathrm{g}} + \dfrac{s}{\omega_{\mathrm{b}}} L_{\mathrm{g}} & -\omega_1 L_{\mathrm{g}} \\ \omega_1 L_{\mathrm{g}} & r_{\mathrm{g}} + \dfrac{s}{\omega_{\mathrm{b}}} L_{\mathrm{g}} \end{bmatrix} \tag{28}$$

The IM $\mathbf{Z_T}(s)$ of the transformer (Fig. 1) in the dq synchronous rotation coordinate system will not be described in detail here, since it is similar to the AC grid IM.

According to the system in Fig.1, it can be seen that the impedances of the D-PMSG, the transformer, and the grid connection are in series. Therefore, the IM of the D-PMSG-GCS in the dq coordinate system is

$$\mathbf{Z_M}(s) = \mathbf{Z_{wv}}(s) + \mathbf{Z_g}(s) + \mathbf{Z_T}(s) \tag{29}$$

where $\mathbf{Z_M}(s)$ is a 2∗2 order impedance matrix.

IV. ESTABLISHMENT OF INM FOR LARGE-SCALE D-PMSG BASED WPGS

With the large-scale access of WTs, large-scale D-PMSG based WPGSs are formed, each of which contains multiple wind farms. The system which is similar to a "single-machine-infinite-bus" shown in Fig. 1 can not reflect the effects of the network topology, the distributed wind speed, and other factors on the SSO characteristics in an MWFGS. In order to solve such problems, an INM is constructed according to an actual network topology of MWFGS. With the system in Fig. 4 as an example, WF1, WF2, WF3 and WF4 are four wind farms (WFs). The wind power generated by the WFs is sent to a 220kV booster transformer via their respective transmission lines (Line$i$ i = 1...4), and then, is transmitted to the main grid via Line0.

A. IM OF WF

Each point of a WF access in Fig. 4 is assumed to be a PV node, while considering the active power of the WF is determined only by the wind speed. If the D-PMSG controller

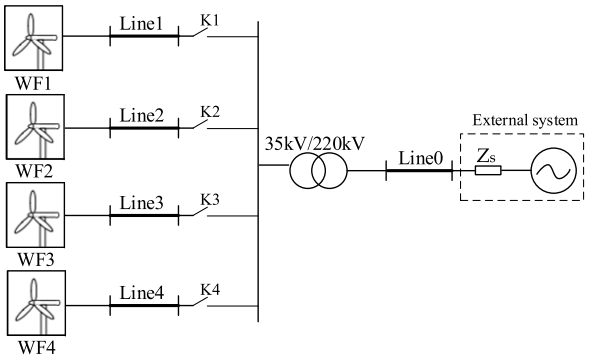

FIGURE 4. MWFGS topology example.

parameters and operating conditions in the equivalent aggregated WF are the same, the impedance model of each WF is

$$\mathbf{Z}_{\mathrm{WF}}(s) = \mathbf{Z}_{\mathrm{wv}}(s)/n \tag{30}$$

where n is the number of WTs included in the WF.

B. IM OF TRANSMISSION LINE

The impedance model of a transmission line in Fig. 4 is equivalent to a π-type equivalent circuit as shown in Fig. 5, where R_{L}, L_{L}, and C_{L} are the lumped resistance, the inductance, and the shunt capacitance, respectively. In general, the effect of the shunt capacitor on the SSO characteristics is very small [23], so it can be ignored.

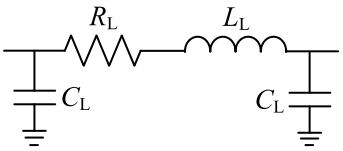

FIGURE 5. Transmission line model.

Similar to (28), the IM of a transmission line in the dq synchronous rotation coordinate system can be presented in (31).

$$\mathbf{Z}_{\mathrm{Line}}(s) = \begin{bmatrix} R_{\mathrm{L}} + \dfrac{s}{\omega_{\mathrm{b}}}L_{\mathrm{L}} & -\omega_1 L_{\mathrm{L}} \\ \omega_1 L_{\mathrm{L}} & R_{\mathrm{L}} + \dfrac{s}{\omega_{\mathrm{b}}}L_{\mathrm{L}} \end{bmatrix} \tag{31}$$

C. IMS OF THE EXTERNAL SYSTEM AND THE TRANSFORMER

The connecting point of the external system (grid) is designated as a $V\theta$ node. The IM of the external system $\mathbf{Z}_{\mathrm{s}}(s)$ is derived with the Thevenin equivalent circuit.

$\mathbf{Z}_{\mathrm{T}}(s)$ is the impedance of the booster transformer.

The IM of the external system $\mathbf{Z}_{\mathrm{s}}(s)$ and the IM of transformer $\mathbf{Z}_{\mathrm{T}}(s)$ are similar to (28).

D. INM OF MWFGS

An MWFGS includes multiple wind farms, transmission elements such as transmission lines and transformers, and external systems. An INM for an MWFGS is constructed with the IMs of all components according to the interconnection topology of them.

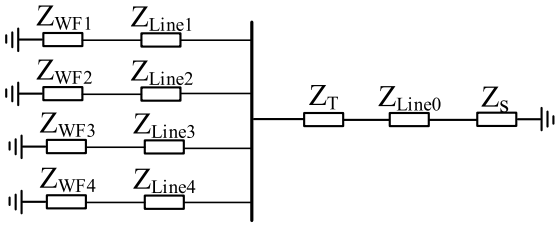

FIGURE 6. INM of the MWFGS.

The example of an MWFGS based on D-PMSG is shown in Fig. 4. Assume that K1-K4 switches are all closed, the INM of the system is established shown in Fig. 6. The INM is further aggregated into lumped impedance as follows.

$$\mathbf{Z}(s) = \mathbf{Z}_1(s) \parallel \mathbf{Z}_2(s) \parallel \mathbf{Z}_3(s) \parallel \mathbf{Z}_4(s) + \mathbf{Z}_0(s) \tag{32}$$

where the symbol "||" stands for the parallel manipulation, $\mathbf{Z}_0(s) = \mathbf{Z}_{\mathrm{T}}(s) + \mathbf{Z}_{\mathrm{Line0}}(s) + \mathbf{Z}_{\mathrm{s}}(s)$, $\mathbf{Z}_1(s) = \mathbf{Z}_{\mathrm{WF1}}(s) + \mathbf{Z}_{\mathrm{Line1}}(s)$, $\mathbf{Z}_2(s) = \mathbf{Z}_{\mathrm{WF2}}(s) + \mathbf{Z}_{\mathrm{Line2}}(s)$, $\mathbf{Z}_3(s) = \mathbf{Z}_{\mathrm{WF3}}(s) + \mathbf{Z}_{\mathrm{Line3}}(s)$, $\mathbf{Z}_4(s) = \mathbf{Z}_{\mathrm{WF4}}(s) + \mathbf{Z}_{\mathrm{Line4}}(s)$. $\mathbf{Z}_{\mathrm{WF1}}(s)$, $\mathbf{Z}_{\mathrm{WF2}}(s)$, $\mathbf{Z}_{\mathrm{WF3}}(s)$ and $\mathbf{Z}_{\mathrm{WF4}}(s)$ are the IMs of the WFs based on D-PMSG WF1, WF2, WF3, and WF4, respectively. $\mathbf{Z}_{\mathrm{line}i}(s)$ $(i = 0, 1 \ldots 4)$ are the IMs of the transmission lines.

V. STABILITY ANALYSIS METHOD

$\mathbf{Z}(s)$ is transformed to $\mathbf{Z}^{\mathrm{m}}(s)$ in the $\alpha\beta$ stationary coordinate system as (33) [8].

$$\mathbf{Z}^{\mathrm{m}}(s) = \mathbf{Z}(s - j\omega_{\mathrm{b}}) \tag{33}$$

The stability of the system depends on the zero point of the determinant of $\mathbf{Z}^{\mathrm{m}}(s)$ [7], which is

$$D(s) = \det(\mathbf{Z}^{\mathrm{m}}(s)) = Z_{\mathrm{dd\text{-}T}}Z_{\mathrm{qq\text{-}T}} - Z_{\mathrm{dq\text{-}T}}Z_{\mathrm{qd\text{-}T}} \tag{34}$$

where $Z_{\mathrm{dd-T}}$, $Z_{\mathrm{dq-T}}$, $Z_{\mathrm{qq-T}}$ and $Z_{\mathrm{qd-T}}$ are the four elements in the second-order matrix $\mathbf{Z}^{\mathrm{m}}(s)$ aggregated from the INM of an MWFGS.

According to the impedance-frequency characteristic curve of $D(s)$, the stability of the SSO mode of the system can be discriminated and the SSO frequency can be quantified [7]. Assume that there is a pair of conjugate zeros in the determinant D(s) within the synchronous frequency range, that is, $\lambda_{1,2} = \alpha_{SSO} \pm j\omega_{SSO}$, and $|\alpha_{SSO}| \ll |\omega_{SSO}|$, when ω is located in the tiny neighborhood of $\lambda_{1,2}$, (34) can be expressed as

$$D(j\omega) = (j\omega - \lambda_1)(j\omega - \lambda_2)G(j\omega) \tag{35}$$

where $G(j\omega) = a + jb$, a, b are constants.

Equation (36) is obtained by separating the real and imaginary parts of $D(j\omega)$ in (35).

$$\begin{cases} \mathrm{Re}[D(j\omega)] = a(-\omega^2 + \alpha_{SSO}^2 + \omega_{SSO}^2) + 2b\alpha_{SSO}\omega \\ \mathrm{Im}[D(j\omega)] = b(-\omega^2 + \alpha_{SSO}^2 + \omega_{SSO}^2) - 2a\alpha_{SSO}\omega \end{cases} \tag{36}$$

The system zero-crossing frequency ω_r can be obtained by making the imaginary part $\mathrm{Im}[D(j\omega)] = 0$, as

$$\omega_{r1,2} = -[\alpha_{SSO}a \pm \sqrt{(\alpha_{SSO}a)^2 + b^2(\alpha_{SSO}^2 + \omega_{SSO}^2)}]/b \quad (37)$$

Since $|\alpha_{SSO}| \ll |\omega_{SSO}|$, there is

$$\omega_r \approx \omega_{SSO} \quad (38)$$

That is to say, the concerned SSO frequency can be obtained by locating the zero-crossing point in the imaginary curve of $D(s)$.

By substituting (37) into (36), the equivalent resistance at the crossing frequency is given by

$$\mathrm{Re}[D(j\omega_r)] \approx (2b\omega_r)\alpha_{SSO} \quad (39)$$

Equation (40) can be obtained from (39).

$$\sigma = -\alpha_{SSO} \approx -\mathrm{Re}[D(j\omega_r)]/(2b\omega_r) \quad (40)$$

where σ is the damping of the SSO.

As can be seen from (40), when the imaginary curve of $D(s)$ crosses ω_r from positive to negative, that is $b > 0$, and $\mathrm{Re}[D(j\omega_r)] < 0$, the SSO is stable; otherwise, it is unstable. When the imaginary curve of $D(s)$ crosses ω_r from negative to positive, that is $b < 0$, and $\mathrm{Re}[D(j\omega_r)] > 0$, the SSO is stable; otherwise, it is unstable.

In order to further quantify the SSO damping, the aggregated RLC circuit method [7], [19], [23] is used. In the tiny neighborhood of the SSO frequency, the impedance model determinant of the system can be equivalent to a complex number multiplied by the impedance of the RLC series circuit. According to the obtained aggregated circuit parameters R and L, the damping of the SSO can be further quantified:

$$\sigma = \frac{R}{2L} \quad (41)$$

VI. CASE STUDY

A. RESEARCH ON THE EFFECT OF WIND SPEED ON SSO CHARACTERISTICS AND D-PMSG IM VALIDATION

The system of a single D-PMSG connected to a grid is shown in Fig. 7. GW/1500, the typical model of D-PMSG used in the WFs in Hami of China, is taken as the research object. The main parameters of the system are given in Table 1.

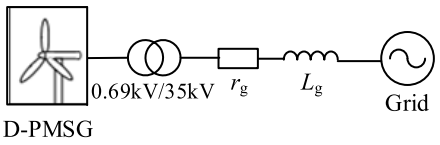

FIGURE 7. A single D-PMSG connected to grid.

1) QUANTITATIVE ANALYSIS OF THE EFFECT OF WIND SPEED ON SSO CHARACTERISTICS

Based on the SSO stability criteria and the calculations of the lumped impedance, the impedance-frequency characteristic curves of the impedance determinant of the single D-PMSG-GCS (shown in Fig. 7) under the different operating wind speed conditions are shown in Fig. 8.

TABLE 1. Parameters of D-PMSG-GCS.

Parameters	Value
Rated power	1.5MW
Rated voltage	0.69kV
DC-side capacitor	C_{dc}=35mF
Filter inductor	L_l=0.4mH
Grid connection reactance	L_g=0.5146H
Grid connection resistance	$r_g = 0$
System's capacity base value	1.5MVA.
DC link rated voltage	1.1kV
Rated wind speed	11 m/s
Cut-in wind speed	3 m/s
Cut-out wind speed	22 m/s

As Fig. 8 shows, the Im curve means the imaginary part of the determinant, the Re curve means the real part of the determinant. In (a) the Im curve crosses the zero point at 21.276Hz from positive to negative while the real part is greater than 0 at the wind speed 3m/s, which means the SSO is unstable. In (b), the Im curve crosses the zero point at 21.077Hz from positive to negative while the real part is greater than 0 at the wind speed 4m/s, which means the SSO is also unstable. When the operating wind speed is 5m/s, the SSO is stable, because the Im curve crosses the zero point at 21.029Hz from positive and negative while the real part is less than 0 in (c). When the operating wind speed is at 6m/s, 7m/s, 8m/s, 9m/s, 10m/s, and 11m/s respectively, the Im curves cross the zero point at 21.122Hz, 21.336Hz, 21.678Hz, 22.178Hz, 22.898Hz, and 23.954Hz from positive and negative while the real parts are all less than zero, in which cases the systems are stable.

In order to quantify the SSO frequency and damping accurately, the IM determinant is further represented by the equivalent RLC circuit near the modal frequency. The SSO frequency and damping of the system under the different operating wind speed conditions are shown in Table 2.

As shown in Table 2 when the wind speed increases, the output power of D-PMSG increases, the damping D increases, and the SSO frequency f_{sub} increases slightly as the same presentation in [2]. Although there is a slight decrease of f_{sub} as the wind speed changes from 3m/s to 5m/s shown in Table 2, it is negligible relative to the overall change trend.

2) VERIFICATION OF D-PMSG IM

Based on the state-space model, the eigenvalue method is used to analyze the case in Fig. 7. The results obtained based on the IM analysis are compared with the results obtained based on the eigenvalue analysis method verified in [18], as shown in Table 3.

It can be seen in Table 3 that at the low wind speeds, SSO frequency obtained by the IM analysis method are close to the results obtained by the eigenvalue analysis method; the errors of the SSO frequency are less than 2%; the deviations

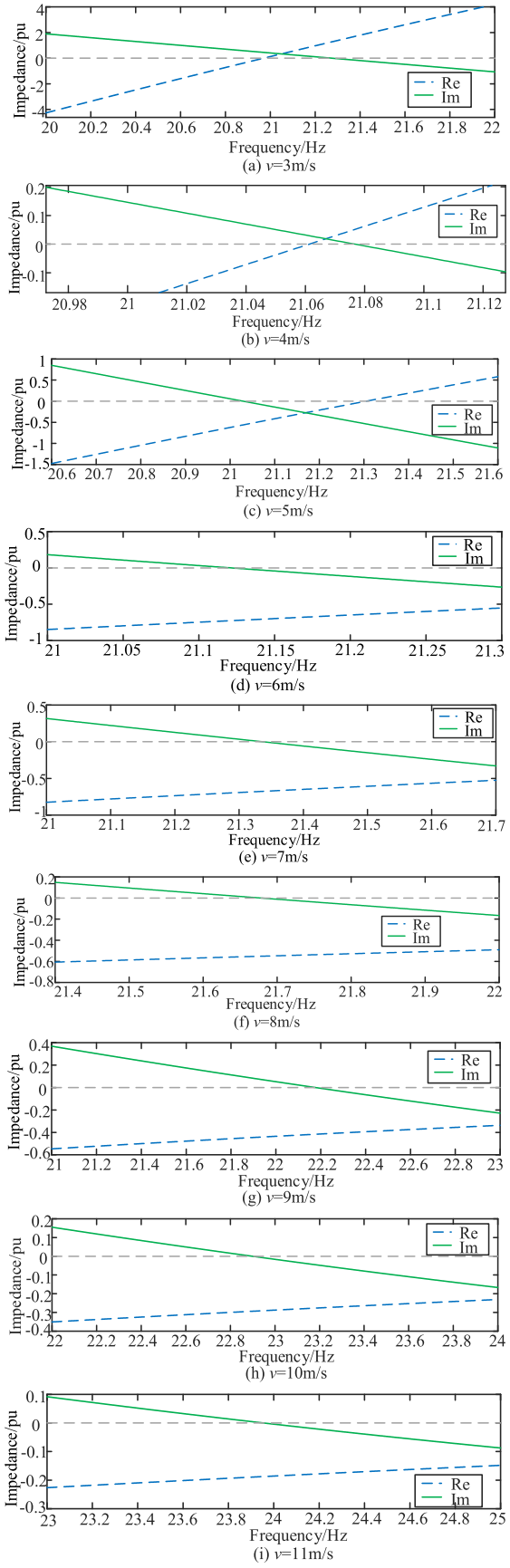

FIGURE 8. Impedance-frequency characteristic curves of the IM determinant of D-PMSG-GCS under different wind speed conditions.

TABLE 2. SSO characteristics under the different wind speeds.

Wind speed (m/s)	P_s (pu)	Frequency f_{sub}(Hz)	Damping D (s^{-1})
3	0.0203	21.276	-3.20
4	0.0481	21.077	-0.18
5	0.0940	21.029	1.79
6	0.1623	21.122	3.05
7	0.2577	21.336	4.57
8	0.3847	21.678	6.58
9	0.5477	22.178	10.22
10	0.7513	22.898	14.49
11	1.0000	23.954	20.29

TABLE 3. Comparison of IM analysis results and eigenvalue analysis results.

Wind speed (m/s)	P_s (pu)	Eigenvalue analysis		IM analysis	
		f_{sub}(Hz)	D (s^{-1})	f_{sub}(Hz)	D (s^{-1})
3	0.0203	21.006	-1.82	21.276	-3.20
4	0.0481	21.005	-1.18	21.077	-0.18
5	0.0940	21.007	-0.11	21.029	1.79
6	0.1623	21.024	1.47	21.122	3.05
7	0.2577	21.075	3.67	21.336	4.57
8	0.3847	21.191	6.58	21.678	6.58
9	0.5477	22.425	10.29	22.178	10.22
10	0.7513	22.859	14.83	22.898	14.49
11	1.0000	23.628	20.19	23.954	20.29

of the damping are a little large, but the trends are consistent. In the range of the high wind speeds, the errors of the damping are small. When the wind speed is between 8m/s and 11m/s, the errors of the damping and the SSO frequency are all less than 2%. Due to the error of input parameters calculated theoretically and the differences of analysis methods, the comparisons of the above results verify the accuracy and the validity of the IM of D-PMSG.

TABLE 4. Impedance parameters of transmission elements and external system.

Parameters	Inductive reactance (Ω)	Resistance (Ω)
Z_s	7.500	0.025
Z_T	6.016	0.040
Line0	5.010	0.030
Line1	0.628	0.030
Line2	0.471	0.030
Line3	0.313	0.020
Line4	0.189	0.010

B. ANALYSIS OF SSO CHARACTERISTICS OF LARGE-SCALE D-PMSGS SYSTEM

1) THEORETICAL ANALYSIS BASED ON INM OF MWFGS

The topology of the MWFGS in Fig. 4 is chosen as the research object. The type of the WTs is GW/1500, and the relevant parameters are shown in Table 1. The impedance parameters of the transmission elements and the external system under the fundamental condition are shown in Table 4. (Z_T is the impedance at 220kV voltage level.)

The WF1, WF2, WF3 and WF4 all contain 175 D-PMSGs with the rated power of 1.5MVA. A time-varying scene is set up for the analysis, which contains the following 4 working conditions.

Working condition 1: In the initial state, K1, K2, K3, and K4 switches are closed. The four farms operate at the same wind speed, 8m/s. The MWFGS operates stably.

Working condition 2: When the MWFGS operates to 30s based on Working condition 1, the operation wind speeds of WF1 and WF2 become 7m/s, and the operation wind speeds of WF3 and WF4 become 6m/s.

Working condition 3: When the system operates to 40s, the operation wind speed of WF4 becomes 3m/s, and the operation wind speeds of other WFs remain unchanged.

Working condition 4: When the system runs to 43s, the operation wind speed of each WF remains unchanged, but the WF4 is cut off.

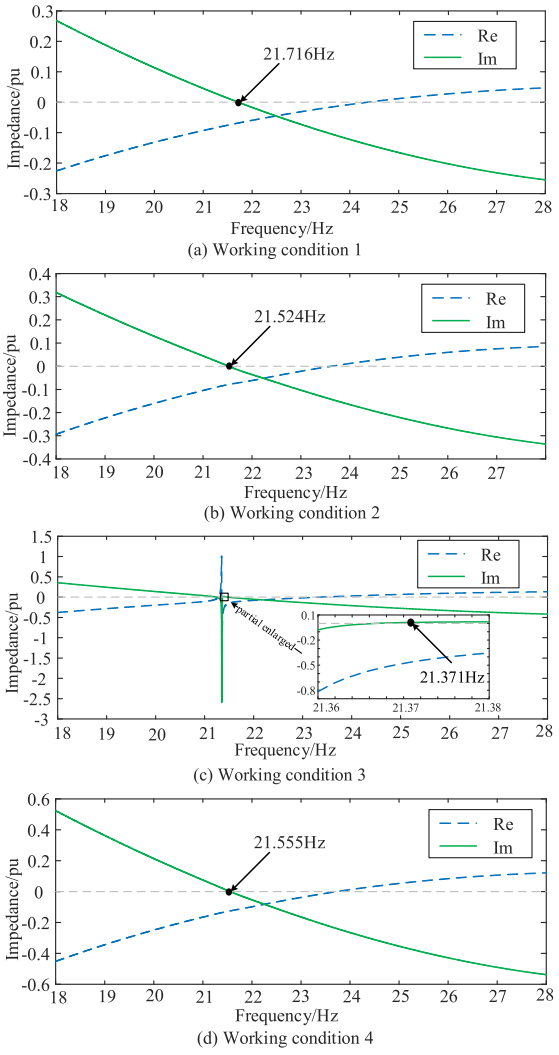

FIGURE 9. Impedance-frequency characteristic curves of INM determinant under the different working conditions.

The impedance-frequency characteristic curves of the determinant $D(s)$ under the different operating conditions are shown in Fig. 9. It can be seen that under condition 1, the zero-crossing frequency is 21.716Hz with the imaginary part of $D(j\omega)$ crossing the zero point from positive and negative, and the real part of the determinant satisfies $\mathrm{Re}[D(j\omega)]<0$, which means the SSO is stable with the positive damping. The SSO damping calculated by the aggregated RLC circuit method is $5.013\mathrm{s}^{-1}$. The working condition 2 is similar to the condition 1, and the SSO frequency and damping of the condition 2 are 21.524Hz and $3.025\mathrm{s}^{-1}$, respectively. Under the working condition 3, the zero-crossing frequency is 21.371Hz with the imaginary part of $D(j\omega)$ crossing the zero point from negative to positive, and the real part of the determinant satisfies $\mathrm{Re}[D(j\omega)]<0$, which means the SSO is unstable with the negative damping, and the SSO damping is calculated as $-0.412\mathrm{s}^{-1}$. Working condition 4 is similar to the working conditions 1 and 2, and the SSO frequency and damping are 21.555Hz and $4.534\mathrm{s}^{-1}$, respectively. It can be seen from the above analysis that the distributed wind speed and the network topology have impacts on the SSO characteristics.

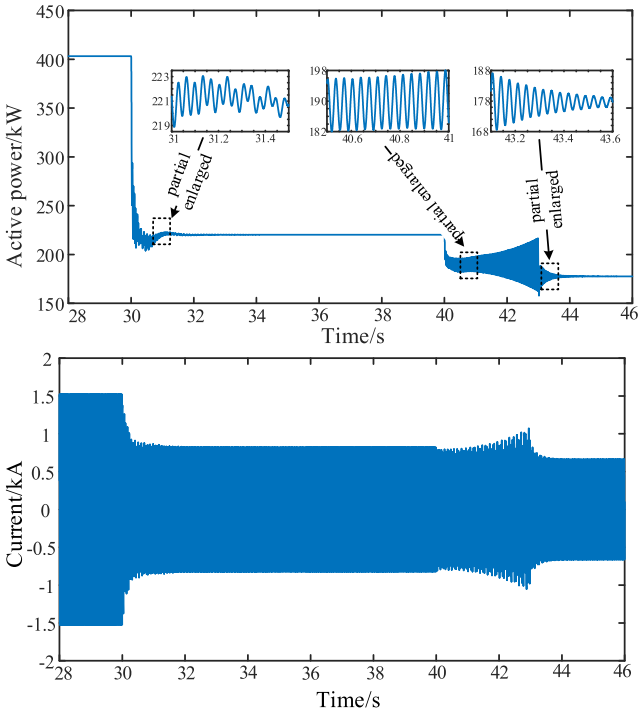

FIGURE 10. Active power and current flowing through Line 0.

TABLE 5. Comparison of the theoretical analysis results based INM and the time-domain simulation results under the different working conditions.

Wind speed (m/s)	Theoretical analysis		Time-domain analysis	
	f_{sub}(Hz)	D (s^{-1})	f_{sub}(Hz)	D (s^{-1})
2	21.524	3.025	21.103	2.651
3	21.371	-0.412	21.071	-0.408
4	21.555	4.534	21.137	4.235

TABLE 6. Comparison of advantages with existing references.

NO.	EXISTING REFERENCES	THIS PAPER
1	[16] considered the voltage outer loop control, but did not quantify the stability of the renewable energy system; [7] proposed a quantitative analysis method for stability, but did not give the expression of corresponding impedance model.	In this paper, the impedance model of D-PMSG considering the effect of the voltage outer loop is established, and the system stability is quantitatively analyzed.
2	[18] quantified the influence of wind speed on the SSO characteristics of D-PMSG based WPGS based on eigenvalue analysis. However, there is no literature to quantify the impact of wind speed on the SSO characteristics of D-PMSG based WPGS with impedance model analysis method.	Based on the impedance model analysis method, this paper quantifies the impact of wind speed on the SSO characteristics of D-PMSG based WPGS.
3	In [23], an INM was proposed to analyze the stability of the sub-synchronous resonance of the multiple wind farms series compensation system, but the impedance model expression of D-PMSG was not presented.	In this paper, the INM of a large-scale D-PMSG-based wind power grid-connected system is established. Based on the INM, the impacts of distributed wind speed and network topology on the SSO stability of the system are quantitatively analyzed.

2) TIME-DOMAIN SIMULATION VERIFICATION

According to the MWFGS shown in Fig. 4, a simulation model is built in the PSCAD/EMTDC to perform the time-domain simulation verification. The curves of the active power and the current flowing through Line 0 are shown in Fig. 10.

As can be seen from Fig. 10, the system is stable in Working condition 1. In Working condition 2, the current and the active power decrease, and reach a stable state after a slight oscillation. In Working condition 3, the current and the active power first decrease, and then rapidly oscillate and diverge. At Working condition 4, the current and the active power decrease, and reach a stable state after a slight oscillation. The stability analysis results based on the time-domain simulation are consistent with the theoretical analysis based on the INM.

Prony analysis is performed on the active power in Fig. 10 to obtain the system's oscillation frequency f_{os} and damping D under Working conditions 2, 3 and 4. The sub-synchronous current oscillation frequency is $f_{sub} = 50\text{-}f_{os}$. The SSO frequencies and dampings of the system under the different operating conditions obtained in the time-domain simulation are compared with the results obtained by the theoretical analysis based on the INM, as shown in Table 5.

It can be seen from Table 5 that under the above three working conditions, the SSO frequencies and dampings of the system obtained by PSCAD time-domain simulation are close to the theoretical analysis results based on the INM, and the SSO frequency errors are all less than 0.5Hz, which verify the accuracy and the validity of the INM.

VII. CONCLUSION

In this paper, an IM of a D-PMSG-GCS is firstly proposed considering the functional relationship between wind speed and wind turbine output power, and the effects of voltage outer loop, current inner loop, phase-locked loop, DC dynamic link, filtering, etc.. Based on the IM of the D-PMSG-GCS, the influences of wind speed on the SSO frequency and damping of D-PMSG are quantified. The accuracy of the IM of D-PMSG is verified by the comparison with the eigenvalue analysis results. Based on the IMs of D-PMSGs and transmission elements, an INM is established according to the topology of the MWFGS. The effects of distributed wind speed and network topology on SSO characteristics are quantitatively analyzed, and the time-domain simulation verifications are performed in PSCAD/EMTDC. The results prove the effectiveness and the accuracy of the INM in analyzing SSO problems of a large-scale D-PMSG-based WPGS. This is of great significance for selection of wind farm locations, parameter settings, and suppression of SSO for large-scale D-PMSG-based WPGSs.

The INM proposed is suitable for small-disturbance stability analysis, because the IM of D-PMSG in INM is established by linearizing at the steady-state operating point. It can be used to study the influences of distributed wind speed, number of wind turbines, network topology and other factors on the stability of SSO. But it is not suitable for the large-disturbance stability analysis, such as faults, dynamic switching and other transient events. The transient problems in large-scale wind power systems need to be further studied.

APPENDIX

See Table 6.

REFERENCES

[1] National Development and Reform Commission of the People's Republic of China. (Mar. 18, 2011). *Medium and Long-Term Development Plan for Renewable Energy [EB/OL]*. [Online]. Available: http://www.cwea.org.cn/policy/dispaly_info.asp?cid=24

[2] X. Xie, H. Liu, J. He, C. Zhang, and Y. Qiao, "Mechanism and characteristics of sub-synchronous oscillation caused by the interaction between full-converter wind turbines and AC systems," *Proc. CSEE*, vol. 36, no. 9, pp. 2366–2372, May 2016.

[3] M. Li, Z. Yu, T. Xu, J. He, C. Wang, X. Xie, and C. Liu, "Study of complex oscillation caused by renewable energy integration and its solution," *Power Syst. Technol.*, vol. 41, no. 4, pp. 1035–1042, Apr. 2017.

[4] Y. Huang, X. Wang, K. Chen, and Y. Huang, "SSI mechanism simulation validation and practical mitigation strategy of DFIG-based wind farm," *Power Syst. Technol.*, vol. 40, no. 8, pp. 2364–2369, Mar. 2016.

[5] X. Dong, X. R. Xie, J. Li, and Y. D. Han, "Comparative study of the impact on subsynchronous resonance characteristics from the different location of wind generators in a large wind farm," *Proc. CSEE*, vol. 35, no. 20, pp. 5173–5180, Jun. 2015.
[6] X. Wang, W. Du, and H. Wang, "Mechanism analysis of instability caused by dynamic interactions between converter control systems in PMSG based wind farms," *Power Syst. Technol.*, vol. 42, no. 8, pp. 2423–2430, Aug. 2018.
[7] H. Liu, X. Xie, G. He, and C. Liu, "Synchronous reference frame based impedance model and stability criterion for grid-connected renewable energy generation gystems," *Proc. CSEE*, vol. 37, no. 20, pp. 4002–4007, May 2017.
[8] M. Cespedes and J. Sun, "Impedance modeling and analysis of grid-connected voltage-source converters," *IEEE Trans. Power Electron.*, vol. 29, no. 3, pp. 1254–1261, Mar. 2014.
[9] C. Zhang, W. Wang, G. He, G. Li, H. Wang, and Y. Tian, "Analysis of sub-synchronous oscillation of full-converter wind farm based on sequence impedance and an optimized design method for PLL parameters," *Proc. CSEE*, vol. 37, no. 23, pp. 6757–6767, Dec. 2017.
[10] X. Wang, L. Harnefors, and F. Blaabjerg, "Unified impedance model of grid-connected voltage-source converters," *IEEE Trans. Power Electron.*, vol. 33, no. 2, pp. 1775–1787, Feb. 2018.
[11] H. Nian and H. Yang, "Impedance modeling and stability analysis of grid-connected inverters under unbalanced operation conditions," *Automat. Electr. Power Syst.*, vol. 40, no. 10, pp. 76–83, May 2016.
[12] H. Xin, Z. Li, W. Dong, L. Zhang, and W. Huang, "Generalized-impedance and stability criterion for grid-connected converters," *Proc. CSEE*, vol. 37, no. 5, pp. 1277–1292, Mar. 2017.
[13] S. Shah and L. Parsa, "Impedance modeling of three-phase voltage source converters in DQ, sequence, and phasor domains," *IEEE Trans. Energy Convers.*, vol. 32, no. 3, pp. 1139–1150, Sep. 2017.
[14] B. Wen, D. Boroyevich, R. Burgos, P. Mattavelli, and Z. Shen, "Analysis of D-Q small-signal impedance of grid-tied inverters," *IEEE Trans. Power Electron.*, vol. 31, no. 1, pp. 675–687, Jan. 2016.
[15] W. Liu, X. Xie, J. Huang, C. Zhang, and C. Yin, "Frequency-coupled impedance model and stability analysis of grid-connected converter," *Automat. Electr. Power Syst.*, vol. 43, no. 3, pp. 138–146, Feb. 2019.
[16] R. Song, J. Guo, B. Li, P. Zhou, and N. Du, "Mechanism and characteristics of sub-synchronous oscillation in direct-drive wind power generation system based on input-admittance analysis," *Proc. CSEE*, vol. 37, no. 16, pp. 4662–4670, Jun. 2017.
[17] Z. An, C. Shen, Z. Zheng, F. Liu, X. Chang, and W. Wei, "Scenario-based analysis and probability assessment of sub-synchronous oscillation caused by wind farms with direct-driven wind generators," *J. Mod. Power Syst. Clean Energy*, vol. 7, no. 2, pp. 243–253, Mar. 2019.
[18] S. Tao, L. Zhao, K. Liao, and Y. Liu, "Probability assessment of characteristics of sub-synchronous oscillation in D-PMSG-based wind power generation system," *IEEE Access*, vol. 7, pp. 133159–133169, Sep. 2019.
[19] H. Liu, X. Xie, C. Zhang, Y. Li, H. Liu, and Y. Hu, "Quantitative SSR analysis of series-compensated DFIG-based wind farms using aggregated RLC circuit mode," *IEEE Trans. Power Syst.*, vol. 32, no. 1, pp. 474–483, Jan. 2017.
[20] P.-H. Huang, M. S. El Moursi, W. Xiao, and J. L. Kirtley, "Subsynchronous resonance mitigation for series-compensated DFIG-based wind farm by using two-degree-of-freedom control strategy," *IEEE Trans. Power Syst.*, vol. 30, no. 3, pp. 1442–1454, May 2015.
[21] L. Fan, R. Kavasseri, Z. L. Miao, and C. Zhu, "Modeling of DFIG-based wind farms for SSR analysis," *IEEE Trans. Power Del.*, vol. 25, no. 4, pp. 2073–2082, Oct. 2010.
[22] L. Wang, X. Xie, Q. Jiang, H. Liu, Y. Li, and H. Liu, "Investigation of SSR in practical DFIG-based wind farms connected to a series-compensated power system," *IEEE Trans. Power Syst.*, vol. 30, no. 5, pp. 2772–2779, Sep. 2015.
[23] H. Liu, X. Xie, X. Gao, H. Liu, and Y. Li, "Stability analysis of SSR in multiple wind farms connected to series-compensated systems using impedance network model," *IEEE Trans. Power Syst.*, vol. 33, no. 3, pp. 3118–3128, May 2018.
[24] S. Huang, J. Gao, and D. Luo, *Direct Drive Permanent Magnet Wind Turbine Design and Grid Control*. Beijing, China: Electronics Industry, 2014, pp. 22–25 and 38–41.
[25] K. Yang and X. Yang, "Small-signal modeling and analysis of grid-connected permnent-magnet synchronous wind generation system," *East China Electr. Power*, vol. 42, no. 9, pp. 1796–1801, Sep. 2014.
[26] W. Liu and J. Jiang, "Modeling and analysis for direct-drive permanent magnet synchronous wind turbine generator in sub-synchronous oscillation," *Motor Control Appl.*, vol. 44, no. 1, pp. 97–103, Jan. 2017.

SHUN TAO (Member, IEEE) was born in China, in November 1972. She received the M.S. and Ph.D. degrees from North China Electric Power University (NCEPU), in 2005 and 2008, respectively.

Since 2008, she has been with NCEPU. She held a postdoctoral position with the Electrical Engineering Laboratory de Grenoble (G2Elab), Institute National Polytechnique de Grenoble (INPG), Grenoble, France, in 2010. Her research interest includes active distribution network and its power-quality.

LEI ZHAO was born in Hengshui, Hebei, China, in 1995. She received the B.S. degree in electrical engineering and automation from Hebei University, Baoding, China, in 2017. She is currently pursuing the M.S. degree with the Institute of State Key Laboratory for Alternate Electrical Power System with Renewable Energy Sources.

Her research interests include power quality and sub-synchronous oscillation in the power system with PMSG.

YUNBO LIU was born in Jilin, China. He received the Bachelor of Engineering degree from the College of Electrical and Electronic Engineering, North China Electric Power University, Beijing, China, in 2018. He is currently pursuing the M.S. degree in electrical engineering with North China Electric Power University.

His current research interests include control systems and power quality of wind power generation.

KUNYU LIAO was born in Xuchang, Henan, China, in 1989. He received the B.S. degree in electrical engineering and automation from the Huazhong University of Science and Technology, Wuhan, China, in 2013, and the Ph.D. degree in electrical engineering from North China Electric Power University, Beijing, China, in 2019.

From 2015 to 2019, he was a Ph.D. student with the Institute of State Key Laboratory for Alternate Electrical Power System with Renewable Energy Sources, Beijing. His research interests include modeling analysis and suppression of power quality and sub-synchronous oscillation in the power system with renewable energy sources.